Power splitters based on the light-intensity-dependent superprism effect

Xiao-Jun Chen, Yi Xu, Sheng Lan, Qi Guo, Xiangbo Yang, and Li-Jun Wu*

Laboratory of Photonic Information Technology, School for Information and Optoelectronic Science and Engineering, South China Normal University, Guangzhou 510006, China

*Corresponding author: ljwu@scnu.edu.cn

Received 22 April 2008; revised 31 July 2008; accepted 8 August 2008; posted 8 August 2008 (Doc. ID 95311); published 5 September 2008

By utilizing the nonlinear Kerr effect of the background medium, power splitters based on the light-intensity-dependent superprism effect are realized in a two-stage system, where two photonic lattices are rotated to each other by 16°. The nonlinear finite-difference time-domain method is applied to conducting numerical experiments. The first lattice acts as the deflecting stage, in which beams with different power densities are separated from each other spatially. The second lattice has a function of "angular amplifier" that enlarges the separation angle between two power density ranges (lower than 100 $W/\mu m^2$ and higher than 300 $W/\mu m^2$) to 90°-like. In the first photonic band, due to the local change of refractive indices induced by the pumping power, new interfaces are formed between the pumped and nonpumped areas. The k-vector will be rotated by these interfaces until the phase velocity and group velocity have the same direction. The shape of the interface between these two stages is discussed. © 2008 Optical Society of America

OCIS codes: 160.5298, 190.4390, 230.1360.

1. Introduction

Photonic crystals (PhCs) [1] have attracted a lot of attention in the past decade due to their ability to control the flow of light on a miniature scale. Many of the studies have focused on new means of tailoring the emission and propagation of light using the photonic bandgap (PBG) property, whereby the photon density of state is zero. On the other hand, outside of the PBG, especially near the PBG, the richness of interesting dispersive properties of the PhC yields one-type device-"passive" devices such as the superprism [2,3], the self-collimator [4], and the polarization beam splitter [5].

The performance of these passive devices continues to excite the community because of their potential application for next-generation photonics technology. The static PhC-based passive devices, however, do not meet the demand for all-optical signal processing in the future. It is desirable to make the effects described above dynamically tunable by introducing an external control to modulate the band structure of the PhC. Depending on the physical properties of the background materials, the tuning of PhCs can be realized by different mechanisms such as varying the temperature [6] and applying an external electric [7] or magnetic field [8] or a mechanical stress [9]. The drawback of these approaches is that they cannot provide all-optical high-speed operability desired for advanced optical signal processing and communication systems [10].

Another method to achieve the tunability is to utilize the nonlinear Kerr effect of the background material in PhCs, whereby the polarizing beam splitter (PBS) is modulated by a pumping beam, either from the top or side of the samples. Since the response is instantaneous, the functionalities realized by PhCs could be greatly enhanced by the addition of Kerr nonlinearities, such as ultrafast all-optical tuning [11], switching [12], and limiting [13]. However, there are only a few studies on introducing the Kerr nonlinearity into passive devices. For example, Nicolea *et al*. have recently demonstrated an optically tunable superprism effect in PhCs with Kerr nonlinearity by means of a modified plane-wave expansion

0003-6935/08/264701-06$15.00/0
© 2008 Optical Society of America

(PWE) method to include the changes of the refractive index induced by nonlinear effects in a self-consistent way [10,14].

The PWE method is well known and has been applied widely to demonstrating the physics underneath the passive device. However, as the nonlinear Kerr phenomenon is a strong local effect and significantly dependent on the local field intensity, the nonlinear finite-difference time-domain (FDTD) method is a more powerful and accurate tool to conduct this kind of numerical experiment than the PWE method is. Not only could the propagating behavior of EM waves in nonlinear PhCs be directly visualized, but also the quantitative result such as the transmission efficiency is easy to obtain.

By utilizing the Kerr effect of the background material, we propose a compact power splitter based on the self-induced superprism effect, where the signal beam acts as the pumping beam so that the power in the signal beam itself is responsible for modifying the PBS. The unifying of the signal beam and the pumping beam enables numerical experiments by a nonlinear FDTD technique. The schematic structure of the device is shown in Fig. 1(a) with two stages operating at two frequencies [see Fig. 1(b)]. The photonic lattices in stage 1 act as the deflecting part based on the superprism effect, while stage 2 acts as an "angular amplifier," to increase the angular separation and thus suppress the crosstalk for a given pumping power spread. The operating frequency in the first stage is chosen as $0.19\,c/a$, a typical operating point for the superprism in the first photonic band (c is the speed of the light, and a is the lattice constant) in order to avoid a complex multimode.

In this paper, both PWE and nonlinear FDTD techniques are utilized to do simulations. PWE with 1764 plane waves is employed to reveal qualitatively the underlying physics of the device. In nonlinear FDTD simulations, a grid size of $a/20$ and a perfectly matched layered boundary condition is used with

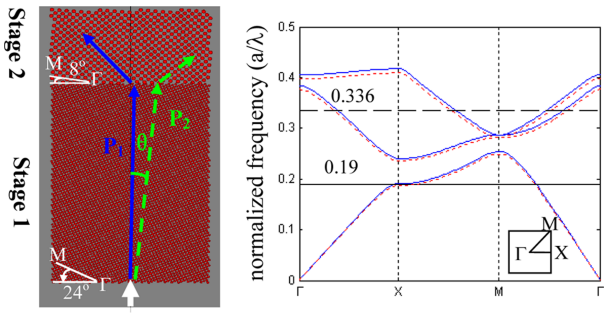

(a) (b)

Fig. 1. (Color online) (a) Schematic structure of the device with two lattices. The gray color denotes the Kerr material and red color the air. (b) Photonic band structure (TM-like mode) for the square PhCs, in which the blue color (solid) curves are for refractive index 2.85 (corresponding to $P/a \sim 100\,\mathrm{W}/\mu\mathrm{m}^2$) and the red color (dashed) for 2.91 (corresponding to $\sim 300\,\mathrm{W}/\mu\mathrm{m}^2$). The straight solid line represents the operating frequency for band 1, and the dashed line is for band 3.

the width of the input Gaussian beam being 8 periods. Pumping power P is the power per unit length in the y direction (parallel to the axis of the holes) with the unit $\mathrm{W}/\mu\mathrm{m}$, and power density P/a ($\mathrm{W}/\mu\mathrm{m}^2$) is the power per unit cell. The time step becomes very important in nonlinear FDTD simulation, as there is no analog of the Courant criterion like in the linear case [15]. To obtain a simulating stability, a smaller time step is required as the material is driven more nonlinearly. We utilized a trial-and-error approach for the highest power density of pumping in this paper ($300\,\mathrm{W}/\mu\mathrm{m}^2$) and found a 1/2 Courant limit is enough to reach the stability. Therefore, a 1/2 Courant limit time step is applied throughout all the nonlinear FDTD simulations.

The basic structure is created by drilling circular air holes in a slab waveguide with the background material being a nonlinear Kerr medium. A two-dimensional (2D) model is sufficient for the purpose, as the photonic functionality depends only on the 2D properties of the lattice. All fields are transverse-magnetic (TM)-like with the E field pointing out of the plane, but a similar case can be constructed for TE-like polarization.

2. Designing the First Stage of the Power Splitter based on the Superprism Effect

In comparison to the triangular and honeycomb PhC structure, a square lattice has a higher asymmetry and results in more aberrance of the dispersion in the low photonic band. We therefore consider a 2D square lattice, with the input interface being rotated 24° away from the ΓM direction, to obtain the sensitive superprism effect [16]. The structural parameter of the PhC is $r/a = 0.34$, where r and a are the hole radius and lattice constant, respectively. The refractive index n_o is assumed to be 2.85, considering bottom cladding materials in the GaAs-based PhC slab waveguide [17], with the nonlinear Kerr coefficient $n_2 = 3 \times 10^{-4}\,\mu\mathrm{m}^2/\mathrm{W}$. Then we have

$$n(x,z) = n_o + n_2 E^2(x,z), \tag{1}$$

where $E^2(x,z)$ is the local electric field intensity. By changing the refractive index $n(x,z)$, the PBS of the PhC could be controlled by an external pumping beam. As the local field intensity is hard to obtain in Kerr nonlinear PhCs, the local refractive index n cannot be precisely defined and is related with the power density P/a approximately. We therefore add "$\sim$" in front of P/a when correlating it with n to show their approximate correspondence.

We start with investigating the relationship between P/a and the deflecting angle θ in the first photonic band near the band edge. Note that the deflecting angle θ in PWE calculation and nonlinear FDTD simulation could be different because of the rotation of the k-vector. This point will be addressed in the following context. In nonlinear FDTD modeling, θ is defined as the angle between the normal to the input interface and the line connecting the first and last

points of the EM waves in the PhCs, as shown in Fig. 1(a). This is different from the definition in the PWE method (the angle between the group velocity and the normal to the input interface). Nonetheless, the results from these two methods are still comparable.

As we know, increasing the refractive index of the medium will drag the PBS to the lower frequency. Consequently, a specific frequency is closer to the band edge in the larger refractive index medium (in the first band), leading to a more sensitive superprism effect. This issue is verified by the dependence of θ on the refractive index of the PhC calculated by the PWE method in Fig. 2(a). As can be seen, with an increase of refractive indices in the background medium, the deflecting angle θ becomes larger. When the refractive index is increased to larger than 2.85, the operating frequency $(0.19c/a)$ approaches to the band edge. Hence, θ starts to increase significantly until this frequency jumps into the photonic bandgap. In order to provide more accurate and convincing results, we then pump the PhC with different power densities to obtain the relationship between θ and P/a by the nonlinear FDTD technique. As expected, higher pumping power densities result in larger refractive indices and thus larger deflecting angles [see Fig. 2(b)]. This is consistent with the results in Fig. 2(a) obtained by the PWE method and could be named as a light-intensity-dependent superprism. It should be noted that, unlike in FDTD modeling, no nonlinear parameters such as pumping power were set during PWE calculation. Only the modification of the refractive index was considered. Therefore, the results from PWE calculation in this paper are direct and only to exhibit the physics of the designed device. FDTD modeling results represent the traveling behavior of EM waves in nonlinear PhCs more accurately than those from the PWE method since the nonlinear effect is greatly dependent on the local field intensity.

Based on this superprism effect, we can then choose two power densities to realize the power splitting. For example, as shown in Figs. 3(a) and 3(c), the beam with power density $300\,\mathrm{W}/\mu\mathrm{m}^2$ refracts to 10° and $100\,\mathrm{W}/\mu\mathrm{m}^2$ to 3°. Therefore these two beams are separated by 7°.

One interesting phenomenon observed in Fig. 3(a) is the rotation of the k-vector. In the linear medium, the way to obtain the direction of the light propagation in the PhC structure is first based on the momentum conservation rule (the component of the input k-vector parallel to the input interface $k_{//} = 0$) and then given by the group velocity $v_g = \nabla_\kappa \omega(\kappa)$, as shown in the dashed black arrow (v_{g1}) in Fig. 3(b). In the nonlinear medium, however, the situation becomes very complicated. If we look closely at the refracted field maps in nonlinear PhCs [Fig. 3(a)], we can see that "wavefronts" (As wavefronts in Bloch waves cannot be defined rigorously, we use double quotation marks here) formed by constant-phase regions are not parallel straight lines (magenta solid lines are given as a visual aid). They are rotating along with the propagating direction. This rotation is likely due to the nonlinearity of the background medium. As we know, in the Kerr medium, the nonlinearity is strongly dependent on the local field intensity. The refractive index will be larger in the higher light intensity area. Consequently, there exist refractive index interfaces between the pumped and nonpumped areas. When the k-vector does not have the same direction as the energy, it will inject into the light intensity-induced interfaces with a slanting angle during the propagation. As a result, the k-vector could be rotated by these local interfaces. The details of these interfaces are hard to obtain since the traveling behavior of the light in nonlinear PhCs is intricate. The overall trend of the resultant rotation, however, is possible to be predicted. The process of the rotation induced by one specific pumping power possibly occurs as plotted in Fig. 3(b): (1) When the pumping power enters into nonlinear PhCs, the group velocity at the very beginning can be obtained by the PWE method like in the

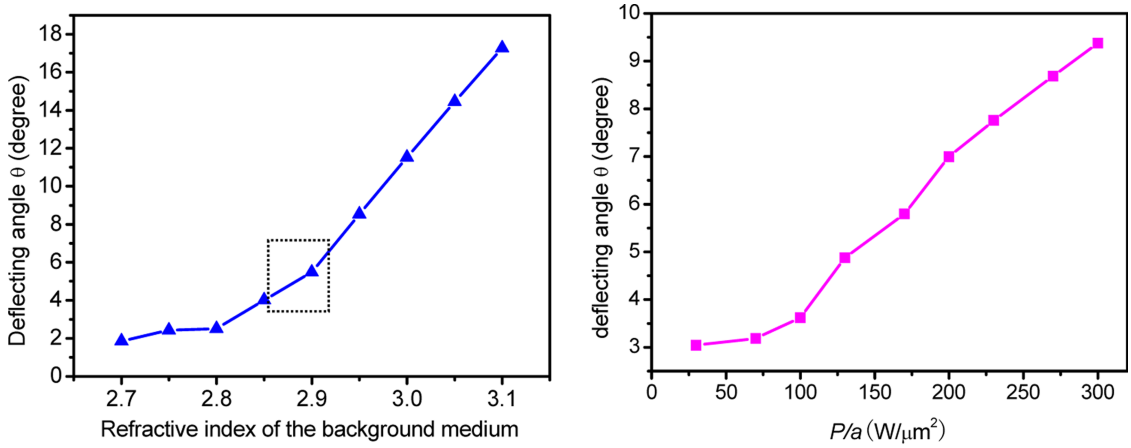

Fig. 2. (Color online) (a) Dependence of the deflecting angle θ on the refractive index of the PhC calculated by the PWE method. The dashed square denotes our operating refractive indices. (b) Relationship between the deflecting angle θ and the input power density obtained by nonlinear FDTD simulations.

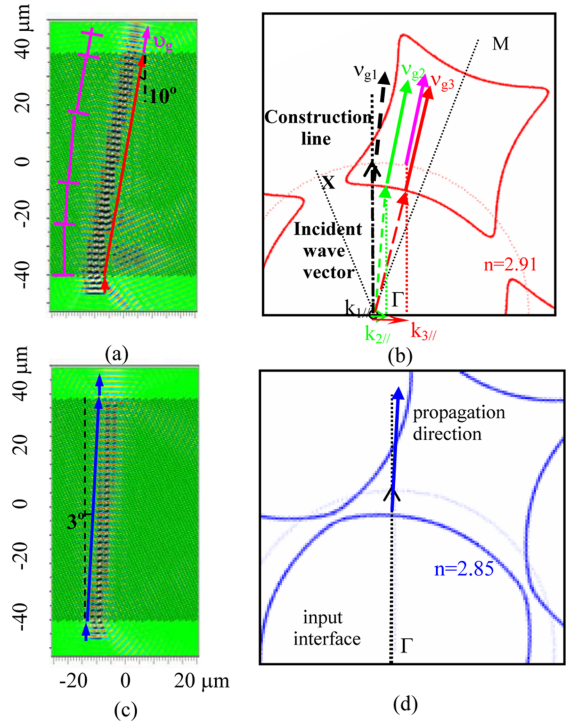

Fig. 3. (Color online) (a), (c) Field distributions of nonlinear FDTD modeling results for power densities of pumping 300 and 100 $\mathrm{W}/\mu\mathrm{m}^2$. The color scale of the filed maps is kept identical throughout this paper. (b), (d) Equi-frequency contours (EFCs) at a frequency of $0.19\,c/a$ for refractive indices of the background material 2.91 (red curves, corresponding to $P/a \sim 300\,\mathrm{W}/\mu\mathrm{m}^2$) and 2.85 (blue curves, corresponding to $\sim 100\,\mathrm{W}/\mu\mathrm{m}^2$).

linear PhC, as shown by the black dashed arrow (ν_{g1}). (2) With the light traveling in the nonlinear PhCs, the local refractive index interfaces induced by the energy come into being. The initial k-vector ($k_{1//} = 0$) experiences these local interfaces with a tilting angle. Therefore, the k-vector starts to rotate, and $k_{//}$ does not equal zero anymore. At the same time, the direction of the group velocity also varies with the rotation of the k-vector. This middle state is displayed in green (ν_{g2} and $k_{2//}$). (3) At last, this rotation is stopped when the k-vector is parallel to the group velocity. There are two factors to influence the rotating process. One is the rotation itself. Along with the rotation, the k-vector departs from the partial gap (in the ΓX direction), and the shape of the equi-frequency contour (EFC) for PhC becomes similar to that for uniform materials. Therefore, the direction of the group velocity approaches that of the phase velocity, as shown in ν_{g3} in Fig. 3(b). On the other hand, the power density decreases with the reduction of the transmission along the propagating direction (due to reflection and scattering losses). As a result, the refractive index of the background medium becomes smaller, and the partial gap on the corresponding EFC is shrinking. Both of these two factors reduce the difference of EFCs between PhC and uniform materials. Therefore the rotation of the k-vector will halt at some point when the direction of the group velocity approaches that of the phase velocity.

3. Designing the Angular Amplifier Stage to Enlarge the Separation between Two Beams

In the above section, the power separation has been realized by two different power densities. The separation angle between two beams, however, is only 7° with 200 $\mathrm{W}/\mu\mathrm{m}^2$ power density difference. A larger spread angle is desirable to suppress the crosstalk and to compact the size of the power splitter at a given difference of P/a.

In this section, we introduce an angular amplifier into the device to enlarge the separation angle between two split beams. This amplifier is also constructed by a square lattice ($r/a = 0.34$), with the input interface being rotated 8° away from the ΓM direction. These two photonic lattices for stages 1 and 2 are therefore rotated to each other by 16°. Figure 4(b) displays the EFCs for frequency $0.336\,c/a$ in the third photonic band with refractive indices 2.85 (corresponding to the pumping power density $\sim 100\,\mathrm{W}/\mu\mathrm{m}^2$) and 2.91 (corresponding to $\sim 300\,\mathrm{W}/\mu\mathrm{m}^2$). It can be seen that the EFCs for both refractive indices are approximately squares with rounded corners (the cusps of the contour). Close to the corner region, the group velocity undergoes a strong shift (90°-like) in the propagation direction when the k vector of the input beam shifts along the interface with a very small angle. In the case of 300 $\mathrm{W}/\mu\mathrm{m}^2$ here, the k-vector has been rotated 10° by stage 1, and the direction of the input k vector for stage 2 is therefore 10°. As $k_{//}$ moves from the left of the cusp to the right, the separation angle for example 7° obtained from stage 1 can be amplified to 90°-like.

It should be noted that the principle to divide two beams by the third band is different from that by the first. In the first band, the separation is realized by the difference of the EFCs for different pumping power densities (refractive indices) at a given input k-vector, as we have pointed out in Section 2. The third band, however, can only amplify the spread angle for

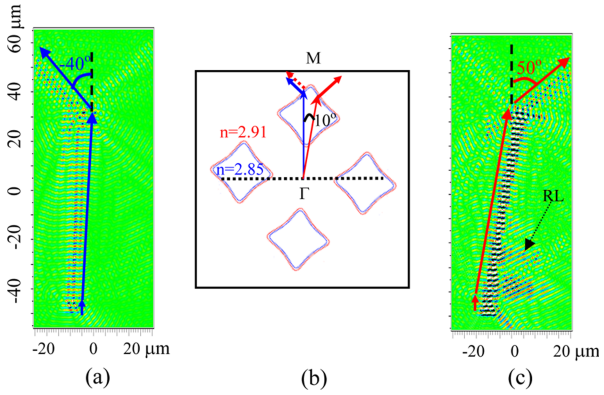

Fig. 4. (Color online) (a) (c) Field maps for the whole device by nonlinear FDTD modeling with $P/a = 100$ and 300 $\mathrm{W}/\mu\mathrm{m}^2$. The structure of the device is exactly the same as shown in Fig. 1(a). Air holes have been deleted to demonstrate the field distribution more clearly. RL in (c) means reflection loss. (b) EFCs at a frequency of $0.336\,c/a$ in the third band for linear PhCs when refractive indices of the background material are 2.91 (red curves, corresponding to the $P/a \sim 300\,\mathrm{W}/\mu\mathrm{m}^2$) and 2.85 (blue curves, corresponding to $\sim 100\,\mathrm{W}/\mu\mathrm{m}^2$).

the already spatially split beams. The basically similar shapes of the EFCs for different refractive indices do not play an important role in this amplification. This can be seen in the left arm of the squarelike shape in Fig. 4(b), where blue solid and red dashed lines show a similar direction of the group velocity. Another point to be noted is the rotation of the k-vector. Unlike in the first band, more than one distinct mode will occur for the same frequency in the third band. Therefore, the definition of the "wavefronts" is much more complex. The discussion of the k-vector rotation in the higher bands is not addressed here.

Figures 4(a) and 4(c) demonstrate the corresponding nonlinear FDTD modeling results. As predicted from PWE calculation, the beam with $P/a = 100\,\mathrm{W}/\mu\mathrm{m}^2$ (300) goes to the −40° (+50°)-like direction, left (right) of the normal to the input interface, meaning that the separation angle is amplified from 7° to 90°-like. The transmittance efficiency (normalized to the source) is 29% for $P/a = 100\,\mathrm{W}/\mu\mathrm{m}^2$ and 20% for $300\,\mathrm{W}/\mu\mathrm{m}^2$. The lower transmission efficiency in Fig. 4(c) is mainly due to the reflection loss (RL), which is induced by the new interfaces between areas with modified and nonmodified refractive indices caused by the external pumping. The crosstalk between the left beam to the right ($P/a = 100\,\mathrm{W}/\mu\mathrm{m}^2$) is 6 dB, while the right beam to the left is 3 dB ($P/a = 300\,\mathrm{W}/\mu\mathrm{m}^2$).

4. Discussion about the Interface between the First and Second Stages

The interface is critical to keep or amplify the k-space distribution for the device. In the linear medium, when the interface between two stages is a straight line and parallel to the input interface (such as in Figs. 4(a) and 4(c)), the k-space distribution would be conserved from one lattice to the next. In such a case, the beam deflected by the first lattice would not be transmitted to the second one, and the spatial displacement in each stage would therefore simply add up rather than the amplification taking place. One way to solve this problem is to rotate the interface between these two stages around the input interface [17]. Figure 5(a) reveals the EFC for the frequency $0.197\,c/a$. In order to hold the output propagating direction as in the PhCs (red solid arrow), the output interface has to be rotated by 40° around the input interface, which is illustrated in the magenta solid line. Figures 5(b) and 5(c) then demonstrate linear FDTD modeling results for the parallel and rotated output interfaces, respectively. As shown, when the output interface for stage 1 is parallel to the input interface, the k-space distribution is conserved, meaning that $k_{//} = 0$ for different frequencies (k-vector direction is exhibited by white arrow), and the direction of the group velocity cannot be kept after the output interface. After rotating the output interface by 40° to the input, the k-vector is rotated by 9° after the output interface, and the direction of v_g is transmitted out of the first lattice, as predicted by the EFC.

In the nonlinear medium, however, the k-space distribution is not conserved anymore. As we have discussed in Section 2, the k-vector is rotated in PhCs by new interfaces between areas with modified and nonmodified refractive indices induced by the external pumping. After rotating to the last direction (when the group velocity and phase velocity have the same direction), the propagating direction of the light is almost conserved when it crosses the flat interface between the PhCs and uniform materials, which is shown by solid magenta and red arrows in Fig. 3(b). By designing the numbers of the periods properly (here we use 80), even with a parallel output interface, the k-vector could be rotated to the same direction as by rotating the output interface in the linear medium. Consequently, the spatial displacement could be amplified by the second stage with a straight line interface between two stages.

5. Conclusions

As the light density has a strong effect on the refractive index of the nonlinear Kerr material, we propose a compact power splitter based on a self-induced superprism effect. The external pumping power could manipulate the beam deflecting from one side to the other. Two photonic lattices rotated to each other by 16° are used to realize the two-stage power splitter. The first lattice acts as the deflecting stage, in which beams with different power are separated from each other spatially. The second lattice has a function of "angular amplifier" that enlarges the separation angle between two power density ranges (lower than $100\,\mathrm{W}/\mu\mathrm{m}^2$ and higher than $300\,\mathrm{W}/\mu\mathrm{m}^2$) to 90°-like. The direction of the interface between these two stages is critical. To transmit the spatial separation of the two beams out of the first lattice, the middle interface has to be rotated by 40° around the input interface in the linear medium. In the nonlinear medium, however, the interface could be a straight line if the number of lattices is designed properly because the k-vector could be rotated by the energy-induced interfaces between the refractive index modified and nonmodified areas in the first photonic band.

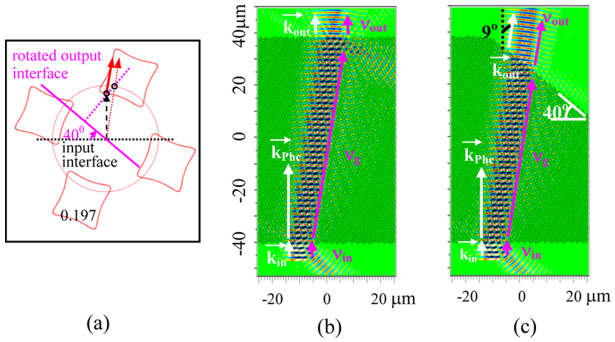

Fig. 5. (Color online) (a) EFC at a frequency of $0.197\,c/a$. To keep the output propagating direction as in the PhCs (red solid arrow), the output interface has to be rotated by 40° around the input interface, which is illustrated by the magenta solid line. (b), (c) Linear FDTD modeling results (frequency at $0.197\,c/a$) for parallel and rotated output interfaces, respectively.

The modeling in this paper is based on a stable state (pumping by the continuous wave). If the pumping is changed to a pulse in the experiment, the situation of the splitting will be more complex. When the power density of the pulse is changed from zero to the peak, the deflecting angle will increase simultaneously, as the response time of the material (Kerr effect) is fast enough to follow this change. When the power density of the pulse is changed from the peak to zero, the deflecting angle will also decrease simultaneously. As the relationship between the deflecting angle and the pumping power density is almost linear when $P/a > 100\,\mathrm{W}/\mu\mathrm{m}^2$, as shown in Fig. 2(b), the deflecting angle will follow the shape of the pulse (if the change of the refractive index induced by the light is not saturated). Therefore the propagating trajectory of the beam in stage 1 will not be a straight line. However, the deflecting still exists in this case when the pumping power is high enough. Two power levels can thus be split spatially by the first stage even with a pulse pumping.

Last, we expect that the power splitter described here can find applications to future optoelectronic devices, such as all-optical switching components or agile light-beam steering systems.

The authors acknowledge financial support from the National Natural Science Foundation of China (grant 10774050) and the Program for Innovative Research Team of Higher Education in Guangdong (grant 06CXTD005). One of the authors (S. Lan) would like to acknowledge financial support by the Program for New Century Excellent Talents (NCET) at the University of China.

References

1. S. G. Johnson and J. D. Joannopoulos, *Photonic Crystals: The Road from Theory to Practice* (Kluwer, 2001).
2. H. Kosaka, T. Kawashima, A. Tomita, M. Notomi, T. Tamamura, T. Sato, and S. Kawakami, "Superprism phenomena in photonic crystals," Phys. Rev. B **58**, 10096–10099 (1998).
3. L. Wu, M. Mazilu, T. Karle, and T. Krauss, "Superprism phenomena in planar photonic crystals," IEEE J. Quantum Electron. **38**, 915–918 (2002).
4. L. Wu, M. Mazilu, and T. Krauss, "Beam steering in planar photonic crystals: from superprism to supercollimator," J. Lightwave Technol. **21**, 561–566 (2003).
5. L. Wu, M. Mazilu, J. F. Gallet, T. Krauss, A. Jugessur, and R. M. De La Rue, "Planar photonic crystal polarization splitter," Opt. Lett. **29**, 1620–1622 (2004).
6. J. Manzanares-Martínez, F. Ramos-Mendieta, and P. Halevi, "Temperature tuning of two-dimensional photonic crystals in the presence of phonons and a plasma of electrons and holes," Phys. Rev. B **72**, 035336–035344 (2005).
7. M. Schmidt, M. Eich, U. Huebner, and R. Boucher, "Electro-optically tunable photonic crystals," Appl. Phys. Lett. **87**, 121110–121112 (2005).
8. M. S. Kushwaha and G. Martinez, "Magnetic-field-dependent band gaps in two-dimensional photonic crystals," Phys. Rev. B **65**, 153202–153205 (2002).
9. W. Park and J. Lee, "Mechanically tunable photonic crystal structure," Appl. Phys. Lett. **85**, 4845–4847 (2004).
10. N. C. Panoiu, M. Bahl, and R. M. Osgood, Jr., "Ultrafast optical tuning of a superprism effect in nonlinear photonic crystals," J. Opt. Soc. Am. B **21**, 1500–1508 (2004).
11. I. Fushman, E. Waks, D. Englund, N. Stoltz, P. Petroff, and J. Vučković, "Ultrafast nonlinear optical tuning of photonic crystal cavities," Appl. Phys. Lett. **90**, 091118–091120 (2007).
12. J. B. Khurgin, "Performance of nonlinear photonic crystal devices at high bit rates," Opt. Lett. **30**, 643–645 (2005).
13. H. Y. Liu, S. Lan, L. Wu, Q. Guo, W. Hu, S. H. Liu, X. S. Lin, and A. V. Gopal, "Self-induced Anderson localization and optical limiting in photonic crystal coupled cavity waveguides with Kerr nonlinearity," Appl. Phys. Lett. **90**, 213507–213509 (2007).
14. N. C. Panoiu, M. Bahl, and R. M. Osgood, "Optically tunable superprism effect in nonlinear photonic crystals," Opt. Lett. **28**, 2503–2505 (2003).
15. M. Bahl, N.-C. Panoiu, and R. M. Osgood, "Nonlinear optical effects in a two-dimensional photonic crystal containing one-dimensional Kerr defects," Phys. Rev. E **67**, 056604–056612 (2003).
16. A. S. Jugessur, L. Wu, T. F. Krauss, and R. M. De La Rue, "Compact and integrated 2-D photonic crystal super-prism filter-device for wavelength demultiplexing applications," Opt. Express **14**, 1632–1642 (2006), http://www.opticsinfobase.org/abstract.cfm?URI=oe-14-4-1632.
17. L. Wu, M. Mazilu, J.-F. Gallet, and T. F. Krauss, "Dual lattice photonic-crystal beam splitters," Appl. Phys. Lett. **86**, 211106–211108 (2005).